Study of the oxidation of a ferritic stainless steel coated with La0.8Sr0.2MnO3 by pulse laser deposition for application in solid oxide fuel cells

Xie, J.; Yoo, Y.; Davidson, I. J.

Publisher's version / Version de l'éditeur:
https://doi.org/10.1149/1.2729018
ECS Transactions, 5, 1, pp. 369-381, 2007

ECS Transactions, 5 (1) 369-381 (2007)
10.1149/1.2729018, ©The Electrochemical Society

Study of the Oxidation of a Ferritic Stainless Steel Coated with $La_{0.8}Sr_{0.2}MnO_3$ by Pulse Laser Deposition for Application in Solid Oxide Fuel Cells

J. Xie*, Y. Yoo and I. J. Davidson

Institute for Chemical Process & Environmental Technology,
National Research Council,
1200 Montreal Road, Ottawa, ON Canada K1A 0R6

* Current Address: Integrated Manufacturing Technologies Institute
National Research Council
800 Collip Circle, London, ON Canada N6G 4X8
Email: jeffrey.xie@nrc-cnrc.gc.ca

The effectiveness in reducing the corrosion of a ferritic (430) stainless steel at moderate and high temperatures by coating it with a thin, dense layer of $La_{0.8}Sr_{0.2}MnO_3$ was investigated. The thin coating of $La_{0.8}Sr_{0.2}MnO_3$ was found to be effective in reducing the growth of oxide scales on the 430 stainless steel. More importantly, the coated steel samples were found to have significantly lower area specific resistances after oxidation treatments than similarly treated uncoated steel samples. The activation energies of the coated steel samples were significantly lower than those of the oxidized bare steel samples for all treatment conditions studied. SEM and X-ray diffraction analyses provided further confirmation that the thin $La_{0.8}Sr_{0.2}MnO_3$ coating is effective in reducing the growth of oxide scale on the surface of the heat treated steel. This study indicates that, cheap and commercially available 430 ferritic stainless steel, with the protection of a thin, dense coating of $La_{0.8}Sr_{0.2}MnO_3$, may be considered as a potential candidate for usage as the interconnect material in solid oxide fuel cells.

Introduction

The interconnect functions as the mechanical and electrical connection between the cathode and anode to form the elements of the fuel cell stack. To be a candidate for the interconnect, a material should meet the following requirements (1-5): high density to avoid mixing of air and fuel, high electrical and negligible ionic conductivity, high thermal conductivity, chemical and physical stability in both oxidizing and reducing environments, a coefficient of thermal expansion well matched to neighboring components, good mechanical strength, acceptable creep resistance at elevated temperatures, ease of fabrication, and low cost.

The trend of decreasing the operating temperature for solid oxide fuel cells, from 1000 °C to 600–800 °C, can significantly increase materials stability and widen the material selection for fuel cell components. In particular, a lower operation temperature makes it possible to use metallic interconnect to replace the ceramic interconnect for planar-type SOFC (6-10). Metallic materials have many advantages compared with the $LaCrO_3$-based ceramic interconnect materials, which include higher thermal and electronic conductivities, good mechanical strength, ease of fabrication and significantly lower cost.

Several kinds of high-temperature alloys (11-16) such as Fe-based alloy, Cr-based heat resistance alloy and chromia-forming alloys have been studied as the metallic interconnect. In general, these candidate alloys contain chromium as alloying element since they form an electronically conductive oxide scale on the surface by preferential oxidation of chromium to chromia (Cr_2O_3) in air as well as in fuel atmospheres. The oxide scale prevents further oxidation of the metallic interconnect. However, at high temperatures chromium oxide generates volatile high-valent Cr-containing species in oxidizing atmospheres. Without effective protective coating, the volatile Cr species causes rapid degradation of the SOFC performance due to the chemical interaction of Cr species at the (La, Sr)MnO_3 (LSM) electrode. Thus, it is important to reduce or inhibit the evaporation of Cr species. One approach is to add some rare earth elements, such as Y, Zr, La and Ce, into the alloy to reduce oxide scale growth rate as well as to increase the electric conductivity of the oxide scale; another is to deposit a dense and electronic conducting coating onto the surface of the alloy to decrease the oxidation rate of the alloy and reduce the Cr vaporization.

As an alternative approach to the bulk modification of alloys, a metallic interconnect can be surface-modified via application of a protective oxide layer on its surface for improved performance (17-22). The protection layer is particularly important at the cathode side due to the oxidizing environment and the susceptibility of SOFC cathodes to chromium poisoning. Functionally, the protection layer is intended first to serve as a mass barrier to chromium cation outward transport. One consequence of the Cr^{3+} outward diffusion is the penetration of chromium into or through the coating, which can lead to the presence of chromium at the coating surface. In air, and particularly in moist air, the surface chromium can react with oxygen and water vapor to form vapor phases and that can migrate into cathodes and degrade cell performance. Secondly the protection layer should be an effective mass barrier to the oxygen anion inward diffusion. As an electrical conduct between adjacent cells, the interconnect and its oxide protection layer(s) have to be electrically conductive. During SOFC operation at elevated temperatures, oxygen ion inward diffusion may lead to a selective oxidation of the substrate alloy and therefore the subsequent growth of a chromia or chromia-rich scale or interlayer between the protection layer and the bulk alloy. Extensive growth of the oxide interlayer may increase the likelihood of spallation, especially during thermal cycling. Thirdly a protection layer is to be more electrically conductive than chromia to minimize the interfacial contact resistance and thus power loss at the cathode/interconnect interface. In addition to the transport properties, thermo-mechanical and chemical stability of the protection layer are essential to maintain its structural integrity during SOFC operation. Accordingly, the candidate materials for the protection layer are also required to have a

good thermal expansion match to the substrate alloy and be thermal-chemically stable and compatible to adjacent stack components in SOFC stacks.

In order to reduce the rate of scale growth on the surfaces of chromia-forming alloys, as well as prevent the chromium vaporization on the cathode side, coating with a perovskite ceramic layer has been suggested and currently is being extensively investigated (23-26). Currently, Sr-doped $LaCrO_3$ (LSC) and $LaMnO_3$ (LSM) are the most favored coating materials, although cheaper substitutes are being sought. In addition to the perovskites, spinel protective layers have also been investigated (27, 28). Overall it appears that the $(Mn,Co)_3O_4$ spinels are promising coating materials to improve the surface stability of ferritic stainless steel interconnects, minimize contact resistance, and seal off chromium in the metal substrates.

LSM-based materials have been investigated as protective coating for chromia-forming alloy interconnect due to its high electrical conductivity and thermal compatibility and stability in oxidizing environment. LSM is also a well known cathode material for SOFC. In the case of LSM coating, the deposition of Cr species is over the whole width of the coating, forming $MnCr_2O_4$ spinel particularly at the outer layer of the coating. Sr enrichment is observed at the interface between the alloy and LSM coating.

In this paper, LSM coating was applied using a Laser Pulse Deposition method. $La_{0.8}Sr_{0.2}MnO_3$-coated 430 stainless steel was investigated and characterized in terms of oxidation behavior, electrical conductivity, and surface characteristics as determined from X-ray powder diffraction and scanning electron microscopy analysis.

Experimental Details

Material and Samples

The ferritic stainless steel selected for this study was 430 stainless steel (430SS), which has a chemical composition (wt) of 16-18 % Cr, max. 1.0 % Mn, max. 1.0 % Si, max. 0.12 % C and Fe for the residual. Steel samples of dimensions of 12 mm ×12 mm ×0.74 mm, were mechanically polished using abrasive papers of from #400 to #1200 grit, and then cleaned ultrasonically in acetone.

Coating of $La_{0.8}Sr_{0.2}MnO_3$

The $La_{0.8}Sr_{0.2}MnO_3$ target was sintered from the commercial powder from Praxair as a disk pellet in a diameter of 15 mm. The $La_{0.8}Sr_{0.2}MnO_3$ films were prepared by pulsed laser deposition (PLD) technique using a KrF excimer laser (Lambda Physik LPX 305i; λ: 248 nm; pulse duration: 25 ns) at an energy of 600 mJ/ pulse (fluence of 1.5 J/cm^2) and a frequency of 8 Hz under a background oxygen pressure of 100 mtorr. The emitted laser beam sputtered the surface of the $La_{0.8}Sr_{0.2}MnO_3$ target for 15 minutes. The coating material was emitted as a vapor and deposited on the surface of 430SS samples. The coating prepared by this procedure is roughly 0.15 μm in thickness.

Oxidation

The oxidation treatments were carried out in a Carbolite tube furnace at temperatures of 600, 700 and 800°C for a period of 72 hours in a flowing air. Comparisons were made of the weight gain from oxidation of bare and coated steel samples. The oxidation weight gains are reported as the difference between the original sample weights and the weights of oxidized steel samples, and divided by the surface area of the samples. Consequently, any losses due to volatization of high valence Cr species are not accounted for.

Electrical Conductivity

The electrical resistances of the coated samples after isothermal heat treatments in air were measured using a four-point DC set up (Figure 1). Uncoated samples were also oxidized in the same conditions and their electrical resistances were measured for comparison. Pt paste was applied by screen printing on the surface of the samples and dried with a blow dryer. The samples were then inserted between two Pt meshes in the electrical conductivity measurement device. A constant DC current of 20 mA was applied using a Keithley 220 power source, the corresponding DC voltage was measured using a Keithley 196 voltmeter.

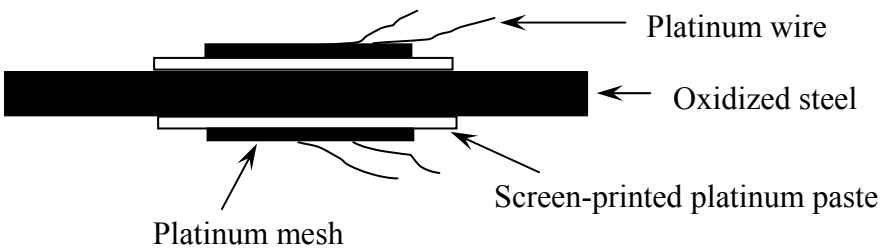

Figure 1. Schematic set-up for the area specific resistance measurement

The electrical resistance is characterized by area specific resistance (ASR), which is defined as:

$$ASR = \frac{V}{I} * S_e \qquad [1]$$

where, V is the DC voltage, I is the constant DC current, and S_e is the area of Pt electrode.

Characterization of the Oxidized Bare and Coated 430 Stainless Steel

A JEOL JSM 5300 scanning electron microscope was used to study the surface morphologies of the bare and coated samples after oxidation, and X-ray powder diffraction using a Bruker D8 diffractometer was employed to analyze the compositions of surface oxides.

Results and Discussions

Oxidation

A comparison of weight gain for bare and $La_{0.8}Sr_{0.2}MnO_3$-coated 430 stainless steel samples after oxidation treatment at temperatures of 600, 700 and 800^0C is plotted in Figure 2. The temperature of the oxidation treatment has a significant influence on the weight gain. The weight gains at 600 and 700°C are in the same order of magnitude, while that after treatment at 800^oC is almost 10 times higher. The coating of $La_{0.8}Sr_{0.2}MnO_3$, even though only around 0.15 μm in thickness, substantially reduces the oxidation weight gain, and the difference between the bare and coated steel is larger at higher temperature. The effectiveness of a coating as a barrier to direct contact between the air and the steel surface depends on its density and thickness. Although, pulsed laser deposition typically produces a coating with very high density, it seems that a thicker coating is required to more effectively reduce the oxidation. However, it can be seen that the application of a perovskite coating by pulsed laser deposition is a promising technique to reduce oxidation of ferritic stainless steels for their application as metallic interconnect materials in solid oxide fuel cells.

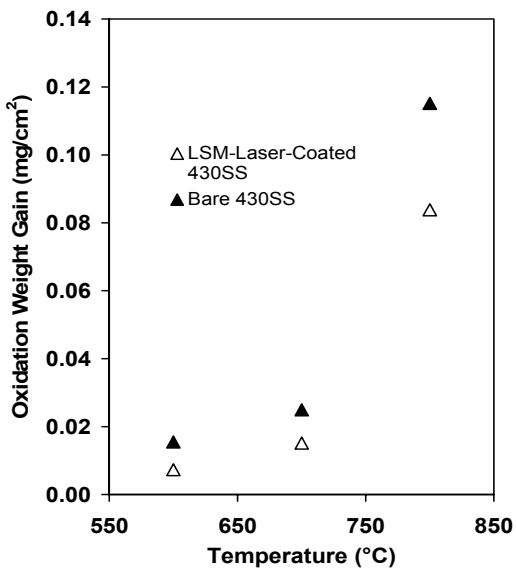

Figure 2. Oxidation weight gain of the bare and coated steels

All the leading candidate alloys for use as interconnects in SOFCs form chromia scales during oxidation. Chromia scales grow by outward diffusion of chromium ions, which can result in the formation of porosity at the alloy–scale interface, and when combined with significant growth stresses, can lead to scale cracking and spallation. At higher temperatures, chromia is oxidized to a gaseous species (CrO_3 or $CrO_2(OH)_2$), which leads to higher oxidation rates as a steady state between scale growth and volatilization is established. The LSM coating behaves as a barrier for outward diffusion of Cr and/or inward diffusion of oxygen, thus reducing the oxidation rate.

Electrical Conductivity

Although oxide scales can provide superior oxidation resistance, they also have much lower electrical conductivities, which lead to unacceptably high resistances when formed at the alloy–electrode interface. The large contact resistance of metallic

interconnects has constituted a major concern due to the drastic drop of the electrical efficiency and premature failure of the stack over the projected service lifetime (40000 h). The contact resistance of an oxidized metallic interconnect is usually characterized by the area specific resistance (ASR), which is the product of electrical resistivity of the studied layer and its thickness, but changes as the interlayer thickness changes, and thus increases with growth of the oxide scale.

For alloys that have been exposed to air at the operating temperature of SOFC for a period of time, oxide scale forms on both sides of the sample. The ASR of such an oxidized alloy can be expressed as:

$$ASR = \tau_s l_s + 2\tau_0 l_0 \qquad [2]$$

where τ_s and l_s are the resistivity and thickness of alloy substrate, respectively, and τ_o and l_o are the resistivity and thickness of oxide scale, respectively. In comparison with the resistivity of the oxide, the resistivity of the metallic substrate is so small that the contribution of the first term in the above equation can be neglected. As such, the ASR of an oxidized metallic interconnect is overwhelmingly dominated by that of the oxide layer on both surfaces so that:

$$ASR = 2\tau_0 l_0 \qquad [3]$$

The ASR of a metallic interconnect is very much influenced by the growth kinetics of the oxide layer upon its long-term exposure to oxidizing atmospheres. Essentially, the oxidation process involves the chemical reaction of a metal with gaseous oxygen in the atmosphere to yield a layer of a protective and thermodynamically stable oxide through either the inward diffusion of oxygen, or the outward diffusion of alloying elements, or both. The thickness of the oxide scale as a function of time (t) at a constant temperature is well documented to obey the general form of:

$$l_0^n = K_p t \qquad [4]$$

where n is an exponent reflecting the oxidation mechanism, and K_p is the a growth rate constant that depends upon the absolute temperature (T) and the activation energy for the diffusion (E_{ox}) of rate-limiting species, and can be empirically represented by the following expression:

$$K_p = K_0 \exp(\frac{-E_{ox}}{kT}) \qquad [5]$$

where K_0 is a pre-exponent constant and k is Bolzmann constant. It has been established that in most cases, the growth of an oxide scale at steady-stage oxidation follows a parabolic behavior, which means that the exponent n in Eq. (4) equals 2 and K_p is often termed as the parabolic rate constant.

Likewise, the conduction of a metal oxide is a thermally activated process that involves the movement of small polarons via the transport of holes (or vacancies). The electrical resistivity which is the inverse of conductivity, can be given as:

$$\tau_0 = \frac{1}{\sigma} = \frac{T}{\sigma_0 \exp(-E_{co}/kT)} = \frac{T}{\sigma_0}\exp(\frac{E_{co}}{kT}) \quad [6]$$

where σ_0 is a pre-exponent constant and E_{co} is the activation energy barrier for the conduction process. Therefore, Eq. (3) can be expressed as:

$$ASR = 2\frac{\sqrt[n]{K_p t}}{\sigma_0} T \exp(\frac{-(1/n)E_{ox} + E_{co}}{kT}) \quad [7]$$

In a situation where the oxide scale thickens in a parabolic fashion, ASR can be expressed as:

$$ASR = \frac{2\sqrt{K_p t}}{\sigma_0} T \exp(\frac{-0.5E_{ox} + E_{co}}{kT}) \quad [8]$$

The relationship of ASR and temperature depends on the relative activation energy of the oxidation and the conductivity processes. It is generally assumed that the resistivity of the substrate alloy is negligible compared with that of the thermally grown scale or pre-applied coatings on the surface of the alloys. As a result, the measured ASR includes that of the scale and/or coating and its interfaces with the substrate and the Pt electrode. Since the current (20mA) applied is relatively small, interfacial polarization is also negligible. Therefore, the measured ASR values, shown in Figure 3, are assumed to be that of the scale and/or coating. Due to improved oxidation resistance, the growth rates of oxide scales on the surfaces of the coated stainless steel samples are much less than those on the bare steel samples. Consequently, the conductivity of the coated steel samples is much higher than those of the bare steel samples. A linear relation is found between log(ASR/T) and 1/T, and the ASR values increase with increasing oxidizing temperature. The difference in ASR between the bare and coated steel samples is small at 600°C and increases dramatically from 700°C. The increases in ASR with increasing temperatures are large for bare steel samples but not for the coated steel samples. For the bare steel samples, the differences (percentage of increase) between ASRs are greater than the changes in the weight gains on oxidation at the specific temperatures studied, indicating that the amount of oxide scale growth is not the sole controlling parameter for ASR in the case of the bare steel samples.

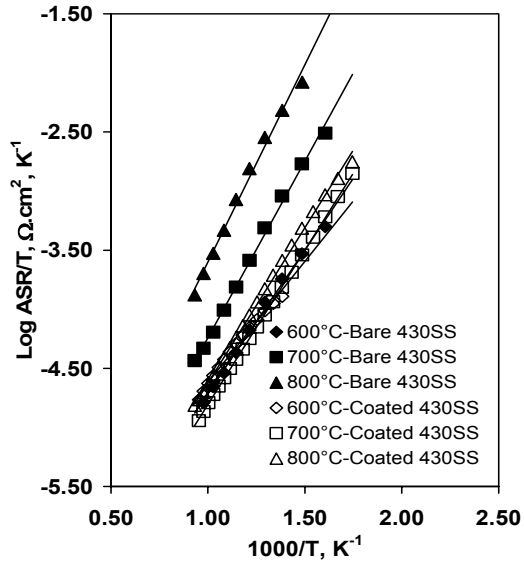

Figure 3. The area specific resistance of the oxidized bare and coated steels

The ASR values of all the coated samples are very similar and similar to that of bare steel oxidized at 600°C/72h, illustrating that the dense and thin PLD-applied coating is very effective to prevent the generalized growth of oxide scales that would interfere with the conductivity. Thus the electrical conductivity of the coated samples remains similar to that of the bare steel at oxidized at 600°C for 72h which indicates that the degradation in electronic conduction during the oxidation is not significant for the coated samples.

By plotting ASR/*T* versus 1/*T* on a logarithmic scale, the activation energy term comprising the contributions of both oxidation and conduction can be attained. It can be readily seen that the ASR changes in a parabolic manner with time at a fixed temperature. In principle, metals that develop slow-growing oxide scale with high electronic conductivity are highly preferred for interconnects. From the slope of the linear relationship between the ASR and the temperature, the activation energy can be obtained (Figure 4). The activation energy of the oxidized bare steel is linearly related to the oxidizing temperature, indicating that the combination of thickness and conductivity (with different phases, identified by XRD, having different conductivities) which contribute to the resistance of the oxide scale varies linearly with treatment temperature. This suggests that the oxide scale on the surface is uniform in its properties. The activation energy for the coated sample is very small at 600°C due to the reduced amount of oxide scale growth and the fact that the $La_{0.8}Sr_{0.2}MnO_3$ coating develops some cracks on heat treatment (Figure 5a), which provide an easy path for conductivity. While the cracks fissure further at 700°C (Figure 5b), the easy path for conduction is apparently blocked most probably as a result of oxide growth with the cracks, thus the activation energy increases dramatically. Even though the oxidation weight gains followed similar trends for both the bare and coated steel samples, the weight gains for the coated samples at 700 and 800°C are occurring preferentially at the cracks of the coating (Figure 5c), and not on the coating-covered areas. Thus the coating-covered area has much less oxide scale growth and provides a preferential path for the conductivity, and consequently, the

activation energy of the coated sample treated at 800°C is almost identical to that at 700°C.

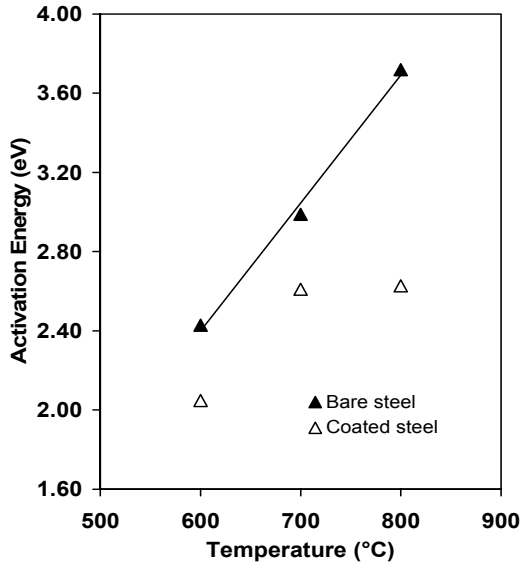

Figure 4. Activation energy of the oxidized bare and coated steels

Characterization of the Oxidized Steel

The morphologies of the uncoated oxidized steel samples, as characterized by SEM, show that the oxidation starts (Figure 6a at 600 °C) at local areas, and then spreads to cover the entire surface (Figure 6b at 700°C and Figure 6c at 800°C) and finally (Figure 6d at 900°C) grows so thick that it starts to crack. In the case of the coated steel samples, cracks can be seen in the coating after heat treatments at 600 and 700°C (Figures 5a and 5b), that are possibly due to a small differential in the coefficient of thermal expansion between the coating and the steel substrate, but there is no evidence of formation of oxide scales on the surface beneath the coating. The oxidation grows preferentially from local areas and these cracks. The thickening of the oxides appearing on the surface after the oxidation at 800°C (Figure 5c) illustrates the patterns of the cracks in the coating.

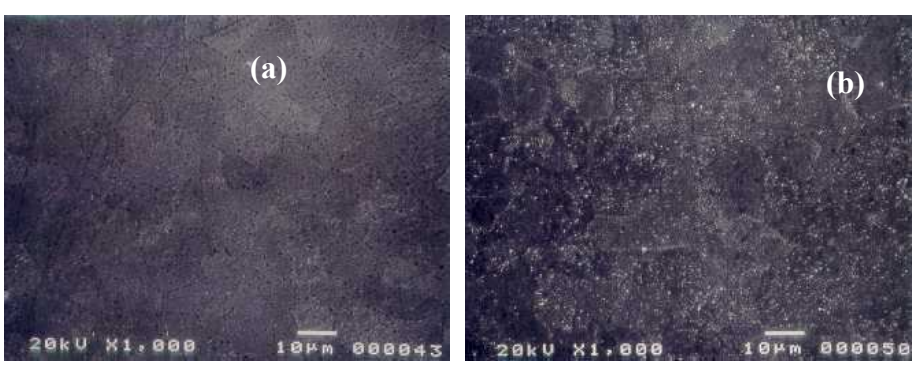

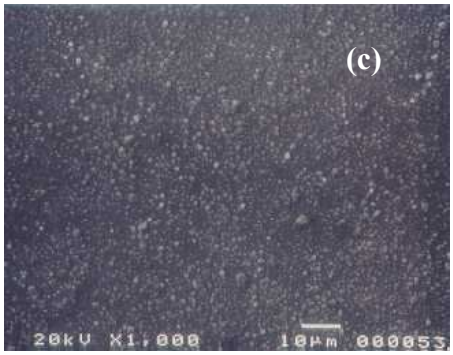

Figure 5. Surface micrographs of coated steel after isothermal oxidation at (a) 600°C, (b)700°C and (c) 800°C for 72 hours

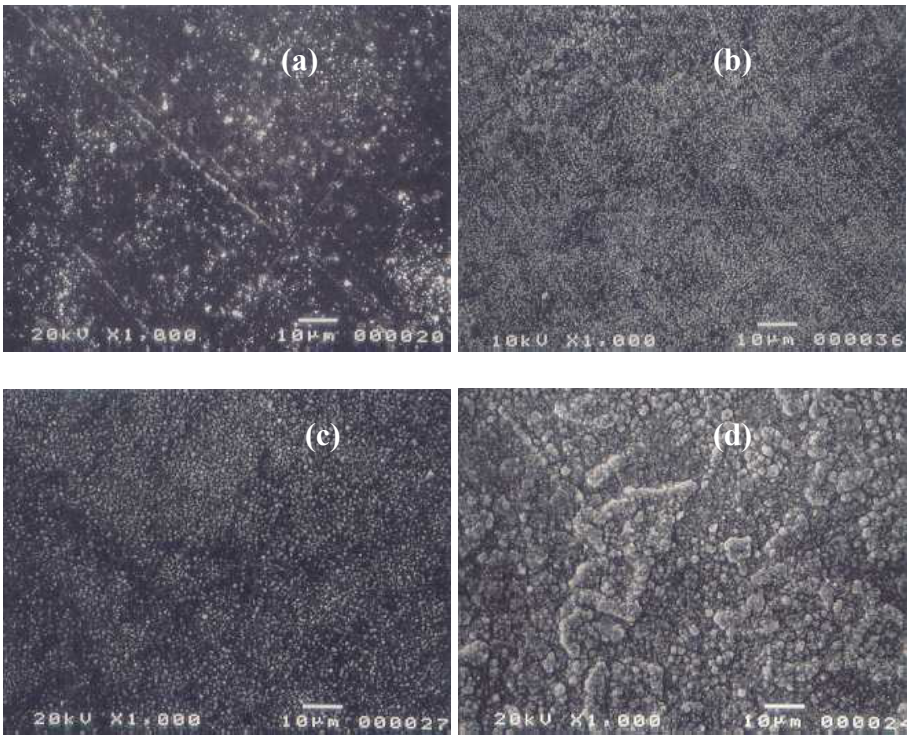

Figure 6. SEM micrographs of the oxidized bare steels at the temperature of (a) 600°C, (b) 700°C, (c) 800°C and (d) 900°C for 72 hours

In the XRD patterns (Figure 7) large amounts of Cr_2O_3 and Cr-Mn-O spinel phases can be seen to cover the surface of the bare steel after oxidation at 800°C, while the $La_{0.8}Sr_{0.2}MnO_3$-coated 430 stainless steel has evidence of only a small coverage of Cr_2O_3 on its surface after oxidation at 800°C. For both the coated and bare steel samples, there is no evidence of oxide scale growth detected in the XRD patterns from the surface of the samples oxidized at 600 or 700°C.

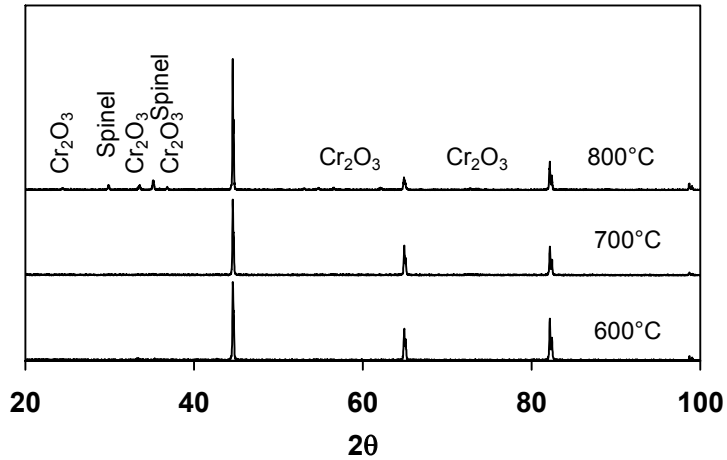

(a)

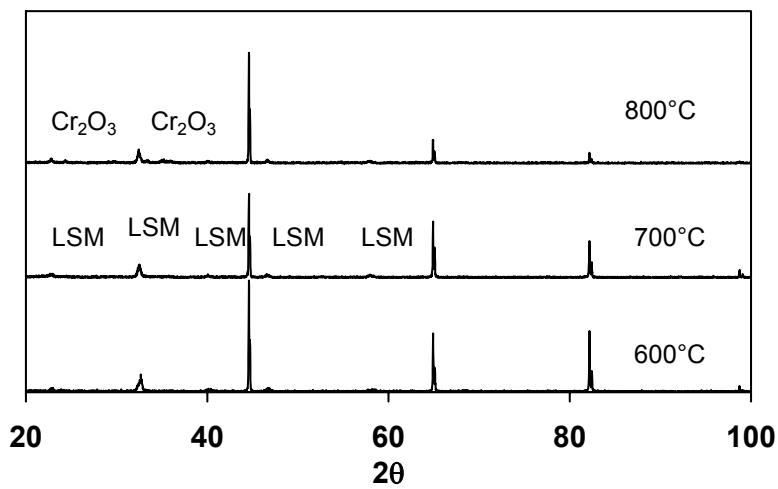

(b)

Figure 7. XRD patterns of oxidized (a) bare and (b) $La_{0.8}Sr_{0.2}MnO_3$ coated steels

On bare steel, oxygen activity at the surface is essentially the oxygen partial pressure in ambient air, i.e., ~0.2 atm, if disregarding water vapor or the surface boundary diffusion layer, which is quite thin at 800°C. Given a sufficient Cr concentration in the steel, Cr is selectively oxidized and forms an external Cr_2O_3-based scale. Once Cr_2O_3 is thermally grown into a dense, continuous surface layer, the oxygen activity at the scale/steel interface decreases, and the scale growth slows down and enters into a steady state. During this state, the scale continues to grow by Cr outward diffusion and oxygen inward diffusion across the thermally grown scale, with the Cr inward transport often dominating and the growth following a parabolic relationship. The continuous growth of the scale over long terms may lead to increased stress in the scale and in particular at the scale/steel interface, causing scale spallation and loss of protection against further environmental attack.

Scale spallation is the result of the thickening of scales, caused by an increase in stored elastic strain energy in the scale due to an increase in scale volume. The ability of coatings to limit scale growth is critical and so deposition of defectless coatings is critical. Adding a coating to the chromia/steel system would generally increase the likelihood of

spallation because of the addition of another residually stressed layer on top of the growing chromia scale. If, however, the coating reduces chromia scale growth rates, the net effect could be no change or, if the scale growth is significantly reduced, the effect could be beneficial in preventing spallation. The latter can be achieved by optimizing coating thickness as well as toughness at the coating/scale interface.

Although the vaporization of the chromia scale does not significantly affect the oxidation rate below 1000 °C, it can be detrimental in other ways to fuel cell performance. Chromium-containing vapor species formed from the interconnect material can be electrochemically or chemically reduced at the electrode surface. The resulting deposition can block the active electrode surface and degrade cell performance. The vapor pressures are higher in air so such poisoning is most likely to occur at the cathode. This degradation can be represented by a decrease in cell voltage or an increase (i.e. more negative) in cell overvoltage. It is also showed that, in accordance with the trend in vapor pressures, the amount of degradation decreases with decreasing oxygen partial pressure.

During high temperature oxidation, outward diffusion of metal cations such as Cr, Ti and Mn ions is simultaneously accompanied by inward diffusion of oxygen anions across a thermally grown oxide scale. Since metals or alloys typically have an appreciable solubility for oxygen, oxygen can dissolve into the alloy substrate near the oxide scale through diffusion along the fast diffusion paths such as grain boundaries, and react with the alloying elements that have higher oxygen affinity to form an internal oxidation zone.

Conclusions

A thin coating of $La_{0.8}Sr_{0.2}MnO_3$ deposited by pulse laser deposition has been shown to dramatically reduce the degradation of the area specific resistance of 430 stainless steel on oxidation at temperatures from 600 to 800°C. Even though oxidation does occur at local points and at the cracks which formed in the coating on isothermal heating, the coating is effective as a barrier to spread of the oxide, and consequently, a low area specific resistance is maintained even after oxidation at 800°C for 72 hours.

The area specific resistance of the bare steel is controlled by the oxides on the surface, in which different phases co-exist and whose thickness increases with increasing temperature, thus the activation energies of the samples of oxidized bare steel are linearly increasing with the increasing oxidation temperature. However, for the coated steel samples, the activation energies increase dramatically from 600 to 700°C due to the effects of oxidation along the cracks in the coating, and only slightly from 700 to 800°C due to the high conductivity of compact coating layer. The activation energies of the coated steel samples were significantly lower than those of the oxidized bare steel samples at all of the treatment temperatures studied.

SEM and XRD analyses show that the thin $La_{0.8}Sr_{0.2}MnO_3$ coating is effective in reducing the formation of oxides on the surface of 430 stainless steel.

Although further optimization of the coating is needed, this study has shown that cheap and commercially available 430 ferritic stainless steel, with the protection of a thin,

dense coating of $La_{0.8}Sr_{0.2}MnO_3$, may be considered as a potential candidate for usage as the interconnect material in solid oxide fuel cells.

Acknowledgements

The authors are very grateful to Ms. Xiaomei Du for the pulsed laser deposition of the $La_{0.8}Sr_{0.2}MnO_3$ coating on 430 stainless steel samples, and to Mr. Gerry Pleizier for the technical support on the SEM analyses.

References

1. W. Z. Zhu, S. C. Deevi, *Mater. Res. Bull.*, **38**, 957 (2003).
2. I. Antepara, I. Villarreal, L. M. Rodriguez-Martinez, N. Lecanda, U. Castro, A. Laresgoiti, *J. Power Sources*, **151**, 103 (2006).
3. J. W. Fergus, *Mat. Sci. Eng.*, **A397**, 271 (2005).
4. C. Hatchwell, N. M. Sammes, I. W. M. Brown, K. Kendall, *J. Power Sources*, **77**, 64 (1999).
5. W. Schafer, A. Koch, U. Herold-Schmidt, D. Stolten, *Solid State Ionics*, **86-88**, 1235 (1996).
6. W. Z. Zhu, S. C. Deevi, *Mat. Sci. Eng.*, **A348**, 227 (2003).
7. T.L Wen, D. Wang, M. Chen, *Solid State Ionics*, **148**, 513 (2002).
8. G. Gabouro, G. Caboche, S. Chevalier, P. Piccardo, *J. Power Sources*, **156**, 39 (2006).
9. T. Brylewski, M. Nanko, T. Maruyama, *Solid State Ionics*, **143**, 131 (2001).
10. E. Ivers-Tiffee, A. Weber and D. Herbstritt, *J. Eur. Ceram. Soc.*, **21**, 1805 (2001).
11. T. Brylewski, K. Przybylski and J. Morgiel, *Mater. Chem. Phys.*, **81**, 434 (2003).
12. S. J. Geng, J. H. Zhu, Z.g. Lu, *Scripta Mater.*, **55**, 239 (2006).
13. Z. Yang, G. Xia, J. W. Stevenson, *J. Power Sources*, **160**, 1104 (2006).
14. S. Geng, J. Zhu, *J. Power Sources*, **160**, 1009 (2006).
15. T. Horita, Y. Xiong, K. Yamaji, *J. Power Sources*, **118**, 35 (2003).
16. K. Hilpert, D. Das, M. Miller, *J. Electrochem. Soc.*, **143**, 3642 (1996).
17. J. H. Zhu, Y. Zhany, A. Basu, Z. G. Lu, M. Paranthaman, *Surf. Coat. Tech.*, **177-178**, 65 (2004).
18. J. W. Fergus, *Mat. Sci. Eng.*, **A397**, 271 (2005).
19. V. I. Gorokhovsky, P. E. Gannon, M. C. Deibert, R. J. Smith, etc., *J. Electrochem. Soc.*, **153**, A1886 (2006).
20. Z. Yang, G. Xia, G. D. Maupin, J. W. Stevenson, *Surf. Coat. Tech.*, **201**, 4476 (2006).
21. H. J. Hwang, S. Lee, E. A. Lee, *J. Am. Ceram. Soc.*, **88**, 3275 (2005).
22. P. E. Gannon, C. T. Tripp, A. K. Knospe, C. V. Ramana, M. Deibert, etc., *Surf. Coat. Tech.*, **188-189**, 55 (2004).
23. Y. D. Zhen, A. P. Jiang, S. Zhang, V. Tan, *J. Eur. Ceram. Soc.*, **26**, 3253 (2006).
24. D. P. Lim, D. S. Lim, J. S. Oh, L. W. Lyo, *Surf. Coat. Tech.*, **200**, 1248 (2005).
25. F. Tietz, I. A. Raj, M. Zahid, D. Stover, *Solid State Ionics*, **177**, 1753 (2006).
26. C. Collins, J. Lucas, T. L. Buchanan, M. Kopezyk, A. Kayani, P. E. Gannon, etc., *Surf. Coat. Tech.*, **201**, 4467 (2006).
27. M. R. Bateni, P. Wei, X. Deng, A. Petric, *Surf. Coat. Tech.*, **201**, 4677 (2007).
28. W. Qu, L. Jian, J. M. Hill, D. G. Ivey, *J. Power Sources*, **153**, 114 (2006).